PROCEEDINGS, 51st Workshop on Geothermal Reservoir Engineering
Stanford University, Stanford, California, February 9-11, 2026
SGP-TR-230

Optimization of Closed-Loop Shallow Geothermal Systems Using Analytical Models

Oliver Heinzel[a], Smajil Halilovic[b], Thomas Hamacher[b], Michael Ulbrich[a]

[a]Technical University of Munich, Chair of Mathematical Optimization, Germany

[b]Technical University of Munich, Chair of Renewable and Sustainable Energy Systems, Germany

Corresponding author: o.heinzel@tum.de

Keywords: Shallow Geothermal Energy, Optimization, Borehole Heat Exchangers, Closed-loop Systems, Ground Source Heat Pump

ABSTRACT

Closed-loop shallow geothermal systems are one of the key technologies for decarbonizing the residential heating and cooling sector. The primary type of these systems involves vertical borehole heat exchangers (BHEs). During the planning phase, it is essential to find the optimal design for these systems, including the depth and spatial arrangement of the BHEs. In this work, we have developed a novel approach to find the optimal design of BHE fields, taking into account constraints such as temperature limits of the heat carrier fluid. These limits correspond to the regulatory practices applied during the planning phase. The approach uses a finite line source model to simulate temperature changes in the ground in combination with the analytical model of heat transport within the boreholes. Our approach is demonstrated using realistic scenarios and is expected to improve current practice in the planning and design of BHE systems.

1. INTRODUCTION

The growing global need for sustainable energy sources has significantly increased demand for closed-loop shallow geothermal systems over the last decade, particularly those with vertical borehole heat exchangers (BHEs) (Halilovic et al., 2022b; Halilovic et al., 2023a). These systems provide an excellent and environmentally friendly way to heat and cool buildings (Rybach and Eugster, 2010; Spitler and Gehlin, 2015). However, their widespread use and economic viability often depend on keeping drilling costs low, which are directly related to the total BHE length, while simultaneously making sure the system is safe and works well throughout its lifespan (Kavanaugh and Orio, 2008; Hellström, 1995).

Planing an optimal BHE field is a challenging task which involves different areas of physics. Full-scale numerical models, like those that use finite element or finite difference methods (Florides and Kalogirou, 2007; Halilovic et al., 2022a), can accurately simulate ground heat transfer, yet they are often too expensive to use in iterative optimization loops (Eskilson, 1987; Halilovic et al., 2023b; Halilovic et al., 2024). To address these computational challenges, modular simulation environments like the Modelica Buildings Library (Wetter et al., 2014) have implemented efficient base classes for calculating thermal response factors, allowing for the dynamic simulation of large-scale borehole fields without the overhead of full-scale discretized models. While temperature response functions, or g-functions, remain the only feasible method for long-term whole-building energy simulations, recent studies using open-source tools such as pygfunction (Cimmino and Bernier, 2014) have shown that managing the computational time and memory requirements for larger fields, often exceeding 100 boreholes, continues to present significant practical challenges (Spitler et al., 2020). Moreover, traditional analytical solutions for BHE sizing frequently utilize notable simplifications that often neglect the complex, dynamic thermal coupling between the circulating heat carrier fluid and the neighboring soil (Yavuzturk and Spitler, 1999). These simplifications can make it more difficult to establish accurate predictions about how the system will work over time and may even lead to designs that do not meet operational needs over the system's lifetime. A significant limitation of existing design tools for BHEs is their restricted capability to accommodate complex, non-convex site geometries (Sanner and Hellström, 1997; Peere and Blanke, 2022). Conventional methodologies predominantly rely on rigid rectangular or regular grid layouts, which often result in suboptimal land utilization or necessitate labor-intensive manual adjustments when confronted with irregular property boundaries, internal obstacles, or building footprints. To overcome these geometric constraints, this study explores a more flexible spatial optimization framework based on Centroidal Voronoi Tessellations (CVTs). Lloyd's algorithm (Lloyd, 1982) remains the foundational iterative procedure for approximating such tessellations; while originally developed for signal quantization, it has proven highly effective in modern practical applications requiring efficient spatial distribution, ranging from the autonomous deployment of multi-robot swarms (Santos et al., 2019) to the coverage optimization of wireless sensor networks (Zhu et al., 2021). In light of these difficulties, this paper seeks to create a computationally efficient and geometrically adaptable optimization framework for BHE field design. The specific goals of this work are threefold:

- To make a quick, analytical model that can predict how well the BHE system will work over a 20-year period, specifically for the 1U-tube BHE setup, which is widely used. This model will be the main part of our optimization loop.
- To present a robust heuristic approach, derived from an adapted Lloyd's algorithm, capable of autonomously identifying optimal BHE coordinates within any non-convex domain, thereby maximizing inter-borehole spacing and distance from domain boundaries.
- To combine the above parts into an optimization problem that minimizes the uniform length of BHEs while strictly following the critical fluid temperature limits ($T_{\min}$ and $T_{\max}$) for the whole simulation period, making sure that the heat pump works safely and efficiently.

2. MATHEMATICAL MODELING

2.1 Soil Temperature Model

We examine the heat transfer within the subsurface, modeled as a homogeneous porous medium. Assuming the absence of groundwater advection, the evolution of the soil temperature change u in space $\mathbf{x}$ and time t induced by a field of vertical BHEs is governed by the classical heat diffusion equation (Carslaw et al., 1948):

$$\partial_t u(\mathbf{x},t) - \alpha \Delta u(\mathbf{x},t) = \frac{\alpha}{\lambda} f(\mathbf{x},t), \tag{1}$$

where α represents the thermal diffusivity and λ denotes the thermal conductivity of the soil. The source term f models the boreholes as finite line sources of the length L, positioned at coordinates $\mathbf{p}$ in the horizontal plane. The heat injection/extraction rate per unit length, q, varies with time. To rigorously satisfy the semi-infinite geometry of the ground while enforcing a constant temperature Dirichlet boundary condition at the surface ($z = 0$), we employ the Method of Images (Carslaw et al., 1948). Mathematically, this is represented in the source term by extending the domain to include a fictitious sink of equal magnitude but opposite polarity, located symmetrically above the ground surface ($z \in [-L, 0]$):

$$f(\mathbf{x},t) = q(t)\left[\mathbb{1}_{[0,L]}(z) - \mathbb{1}_{[-L,0]}(z)\right]\delta_{\mathbf{p}}(x,y). \tag{2}$$

The fundamental analytical solution is derived by convolving this source distribution with the three-dimensional Green's function (heat kernel) for infinite space (Evans, 2022), given by:

$$\mathcal{G}(\mathbf{x},t) = (4\pi\alpha t)^{-3/2}\exp\left(-\frac{|\mathbf{x}|^2}{4\alpha t}\right).$$

By convolving the Green's function with the vertical line source, we obtain a combination of error functions. We define the resulting vertical response function $\mathcal{Z}$ as:

$$\mathcal{Z}(z,\tau;L) := \frac{1}{2}\left[\mathrm{erf}\left(\frac{L-z}{2\sqrt{\alpha\tau}}\right) + 2\mathrm{erf}\left(\frac{z}{2\sqrt{\alpha\tau}}\right) - \mathrm{erf}\left(\frac{L+z}{2\sqrt{\alpha\tau}}\right)\right] \tag{3}$$

and the corresponding horizontal response function $\mathcal{R}$ as:

$$\mathcal{R}(r;\tau) := \frac{1}{\tau}\exp\left(-\frac{r^2}{4\alpha\tau}\right). \tag{4}$$

Consequently, the temperature variation at any position $\mathbf{x} = (x, y, z)$ and time t is expressed as the temporal convolution of the load history with these spatial kernels:

$$u(\mathbf{x},t) = \frac{1}{4\pi\lambda}\int_0^t q\,(t-\tau)\cdot \mathcal{R}(r(x,y,\mathbf{p});\tau)\mathcal{Z}(z,\tau;L)\,d\tau, \tag{5}$$

where $\mathbf{p} = (p_x, p_y)$, $\quad r(x,y;\mathbf{p}) = \|\,(x,y) - (p_x,p_y)\,\|$ is the radial distance from the borehole axis.

For the specific case where the heat load q is constant or a step function, this temporal convolution is equivalent to the spatial integration form commonly found in literature, named as the Finite Line Source model (Lamarche and Beauchamp, 2007; Molina-Giraldo et al., 2011):

$$u(\mathbf{x},t) = \frac{q}{4\pi\lambda}\left(\int_0^L \frac{\mathrm{erfc}\left(\frac{R(x,y,z;\xi)}{\sqrt{4\alpha t}}\right)}{R(x,y,z;\xi)}\,d\xi - \int_{-L}^0 \frac{\mathrm{erfc}\left(\frac{R(x,y,z;\xi)}{\sqrt{4\alpha t}}\right)}{R(x,y,z;\xi)}\,d\xi\right) \tag{6}$$

with the Euclidean distance $R(x,y,z;\xi) = \sqrt{r(x,y)^2 + (z-\xi)^2}$. It is important to note that the integrands exhibit a singularity as the radial distance $r(x,y) \to 0$; therefore, the solution is valid strictly for evaluation points located at a non-zero radius, such as the borehole wall ($r_b > 0$), rather than at the centerline.

Due to the linearity of the governing heat equation w.r.t. the parameter q, the principle of superposition applies. This allows us to extend the single-source solution to a field of boreholes by summing the contributions of individual Dirac sources $\sum_{k=1}^{N_b} \delta_{\mathbf{p}^k}$. Strictly speaking, a coupled system would result in a distinct heat extraction rate q_k for each borehole. However, we approximate the heat extraction rate as uniform across all boreholes ($q_k \approx q$), neglecting the slight variations that arise in practice. Hence, the total temperature field variation is obtained by summing over all borehole positions $\{\mathbf{p}^k | k = 1, \dots N_b\}$:

$$u(\mathbf{x}, t) = \frac{1}{4\pi\lambda} \sum_{k=1}^{N_b} \int_0^t q\,(t-\tau) \cdot \mathcal{R}(r(x, y; \mathbf{p}^k); \tau) \mathcal{Z}(z, \tau; L)\, d\tau. \tag{7}$$

2.2 Fluid Temperature Model

We treat the depth range $z \in [0, L]$ as the active heat exchanger zone to model the boundary condition at the borehole wall. We use a quasi-steady-state approximation to describe how the circulating fluid and the borehole wall (at temperature $T_b(z,t)$) interact thermally. Neglecting the thermal mass of the fluid, the heat balance for the downward flowing fluid (T_i) and upward flowing fluid (T_o) is dictated by the coupled system of differential equations formulated by (Eskilson and Claesson, 1988) for the 1U configuration:

$$\begin{aligned} \rho^r c^r \dot{m}^r \frac{\partial T_i}{\partial z}(z,t) &= \frac{T_b(z,t) - T_i(z,t)}{R_s} - \frac{T_i(z,t) - T_o(z,t)}{R_{inter}} \\ -\rho^r c^r \dot{m}^r \frac{\partial T_o(z,t)}{\partial z} &= \frac{T_b(z,t) - T_o(z,t)}{R_s} + \frac{T_i(z,t) - T_o(z,t)}{R_{inter}}, \end{aligned} \tag{8}$$

with density ρ^r, specific heat capacity c^r and mass flow rate $\dot{m}$. There are two main thermal resistances in the system R_s, which controls how heat moves between the pipe and the borehole wall, and R_{inter}, which accounts for how heat moves between the two pipe legs. These resistances can be determined experimentally or calculated using approximate analytical expressions based on the borehole geometry, as detailed in (Diersch et al., 2011; Diersch, 2014). This formulation assumes thermal equilibrium within the borehole cross-section (Figure 1). Thus, this description is only true for times $t > 5\frac{r_b^2}{\alpha}$ (Diersch et al., 2011), which gives the grout enough time to stabilize after any temporary changes.

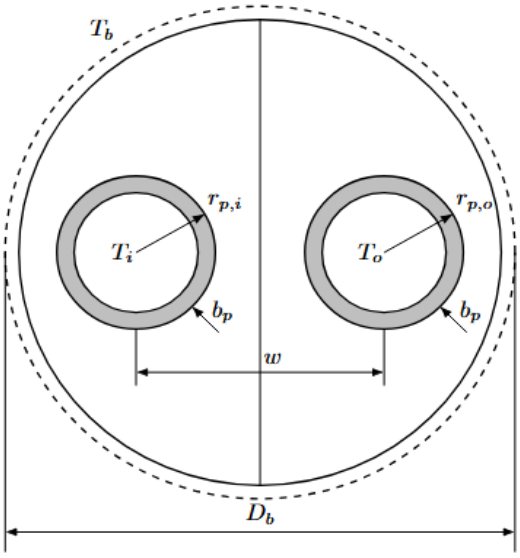

Figure 1: Cross section of a 1U borehole consisting of two pipe components and two grout zones (modified from (Diersch et al., 2011)).

Applying boundary conditions at the top and bottom of the borehole closes the equation system. We set a Dirichlet condition at the inlet ($z = 0$) and a continuity condition at the U-bend ($z = L$) for a given time-dependent inlet temperature $T_{in}(t)$:

$$\begin{aligned} T_i(0,t) &= T_{in}(t) \\ T_i(L,t) &= T_o(L,t). \end{aligned}$$

It is assumed that the pipes are arranged symmetrically within the borehole for standard 1U configurations. This means that both legs have the same soil-to-pipe resistance R_s. The primary quantity of interest is the fluid outlet temperature $T_{out}(t) := T_o(0,t)$. This is the temperature of the fluid leaving the borehole at the surface.

The analytical solution to this system of equations (8), which connects the temperature at the outlet to the temperature at the inlet and the vertical profile of the wall temperature, is found in (Eskilson and Claesson, 1988):

$$T_{out}(t) = T_{in}(t)g_1(L) + g_2(L)\int_0^L T_b(\xi,t)g_3(L-\xi)d\xi \tag{9}$$

The functions $g_1, g_2,$ and g_3 represent the BHE's geometric and thermal properties, which are defined as follows:

$$\begin{aligned} g_1(z) &:= \frac{2\gamma}{\beta_s \tanh(\gamma z)+\gamma} - 1, & g_2(z) &:= \frac{\gamma}{\beta_s \sinh(\gamma z)+\gamma\cosh(\gamma z)}, & g_3(z) &:= 2\beta_s \cosh(\gamma z) \\ \text{where}\quad \beta_s &= \frac{1}{R_s \rho^r c^r \dot{m}^r}, & \beta_{inter} &= \frac{1}{R_{inter}\rho^r c^r \dot{m}^r}, & \gamma &= \sqrt{\beta_s(\beta_s + 2\beta_{inter})} \end{aligned} \tag{10}$$

2.3 Soil-Fluid Coupling Strategy

The system is driven by a given external energy demand E varying in time. The coupling with the fluid loop is defined by the balance equation:

$$E(t) = \dot{m}c_p\big(\langle T_{out}\rangle(t) - T_{in}(t)\big) \tag{11}$$

where $\langle T_{out}\rangle$ denotes the averaged outlet temperatures among the BHEs. We assume a uniform heat extraction rate along the length of each borehole and that these rates are identical for all boreholes in the field. But the average temperatures along the borehole walls are assumed to be unequal. This is due to the varying thermal interference experienced at different spatial positions within the field. This configuration corresponds to BC-I as defined in (Cimmino and Bernier, 2014).

The Dirichlet boundary condition at the BHE walls implies that the soil temperature u at the interface $r = r_b$ dictates the boundary temperature T_b. The thermal influence of a source borehole k on a target borehole $\hat{k}$ is given by:

$$u_{k\to\hat{k}}(z,t) := \frac{1}{4\pi\lambda}\int_0^t q(t-\tau)\mathcal{R}\big(r_{k,\hat{k}},\tau\big)\mathcal{Z}(z,L,\tau)\,d\tau, \tag{12}$$

This formulation is motivated by eq. (7). When considering the self-influence ($k = \hat{k}$), the temperature is computed at the borehole wall radius r_b. Therefore, the radial distance $r_{k,\hat{k}}$ is defined by:

$$r_{k,\hat{k}} = \begin{cases} \| \mathbf{p}^k - \mathbf{p}^{\hat{k}} \| & \text{if } k \neq \hat{k}, \\ r_b & \text{if } k = \hat{k}, \end{cases} \tag{13}$$

where $\mathbf{p}^k$ is the position of the BHE k. To link the soil temperature field to the fluid outlet temperature, we introduce the vertically integrated thermal response, $\hat{u}_{k\to\hat{k}}$ between BHE k and BHE $\hat{k}$ defined as

$$\hat{u}_{k\to\hat{k}}(t;L) := \int_0^L u_{k\to\hat{k}}(z,t)\,g_3\big(\gamma(L-z)\big)\,dz. \tag{14}$$

Physically, this quantity represents the effective temperature influence on the fluid, weighted by the BHE's internal heat transfer characteristics g_3 defined in (10) along the length of the pipe.

Substituting (12) into (14) and applying Fubini's theorem to interchange the temporal and spatial integration yields:

$$\hat{u}_{k\to\hat{k}}(t;L) = \frac{1}{4\pi\lambda}\int_0^t q(t-\tau)\mathcal{R}\big(r_{k,\hat{k}},\tau\big)\hat{\mathcal{Z}}(\tau;L)\,d\tau, \tag{15}$$

where the spatial integral $\hat{\mathcal{Z}}$ admits the following closed-form solution:

$$\hat{\mathcal{Z}}(\tau;L) := \int_0^L \mathcal{Z}(z,\tau;L)\cdot g_3\big(\gamma(L-z)\big)\,dz = \frac{\beta_s}{2\gamma}\mathcal{H}\big(\xi(\tau),\eta(\tau)\big). \tag{16}$$

Here, the auxiliary function $\mathcal{H}$ is defined as:

$$\mathcal{H}(\xi,\eta) = 4\cosh^2(\xi\eta)\mathcal{E}(\xi,\eta) - \mathcal{E}(2\xi,\eta) - \big(1 + 2\cosh(2\xi\eta)\big)\mathcal{E}(0,\eta), \tag{17}$$

with the function $\mathcal{E}$ given by

$$\mathcal{E}(\xi,\eta) = e^{\eta^2}\left[e^{2\xi\eta}\operatorname{erf}(\xi+\eta) - e^{-2\xi\eta}\operatorname{erf}(\xi-\eta)\right] \tag{18}$$

with dimensionless parameters

$$\xi(t) = \frac{L}{2\sqrt{\alpha t}}, \quad \eta(t) = \gamma\sqrt{\alpha t}.$$

By the symmetry of the radial distance matrix, we have $\hat{u}_{k\to\hat{k}} = \hat{u}_{\hat{k}\to k}$ for all $k, \hat{k} = 1, \dots, N_b$. Furthermore, assuming identical borehole geometries, the self-response is uniform across the field, therefore $\hat{u}_{k\to k} = \hat{u}_{1\to 1}$ for all $k = 1, \dots, N_b$.

Combining the soil temperature response (7) with the outlet temperature definition (9), and solving for the inlet temperature T_{in} in the energy balance equation (11), the average outlet temperature of the BHE field is derived as:

$$\langle T_{out}\rangle(t) = \psi_1(L)\left(\Psi_{inter}(t;L) + \Psi_{self}(t;L)\right) + \psi_2(L)\Delta T_{pipe}(t). \tag{19}$$

The coefficients ψ_1 and ψ_2, and the transient pipe temperature drop ΔT_{pipe} are defined as:

$$\psi_1(z) \coloneqq \frac{\gamma\operatorname{csch}(\gamma z)}{2\beta_s}, \quad \psi_2(z) \coloneqq \frac{1}{2}\left(\frac{\gamma\coth(\gamma z)}{\beta_s} - 1\right), \quad \Delta T_{pipe}(t) \coloneqq \frac{E(t)}{\dot{m}c_p}. \tag{20}$$

Finally, the self-response and averaged interaction terms are given by:

$$\Psi_{self}(t;L) \quad \coloneqq \hat{u}_{1\to 1}(t;L) = \frac{1}{4\pi\lambda}\int_0^t q\,(t-\tau)\mathcal{R}(r_b,\tau)\hat{\mathcal{Z}}(\tau;L)\,d\tau, \tag{21}$$

$$\Psi_{inter}(t;L) \quad \coloneqq \frac{2}{N_{bhe}}\sum_{k=2}^{N_{bhe}}\sum_{\hat{k}=1}^{k}\hat{u}_{k\to\hat{k}}\,(t;L). \tag{22}$$

2.4 Temporal Superposition and Aggregation

The heat extraction rate per unit length q is related to the total building energy demand E and the field configuration

$$q(t) = -\frac{E(t)}{LN_b}. \tag{23}$$

In practical applications, E is modeled as a piecewise constant function defined on a uniform temporal grid $t_0, \dots, t_{N_t}$, typically representing hourly or monthly intervals

$$E(t) = \sum_{l=0}^{N_t-1} E_l \cdot \mathbb{1}_{[t_l,t_{l+1})}(t). \tag{24}$$

To accurately capture peak load behavior and ensure system limits are not violated, the simulation requires a fine temporal resolution (e.g., hourly time steps). However, a brute-force calculation of the full temperature field is computationally prohibitive. For a typical simulation horizon of 20 years with hourly steps ($N_t \approx 175{,}200$) and a field of 25 BHEs, a naive approach would require evaluating the convolution integral over 10^8 time steps, scaling with $O(N_t^2 \cdot N_{bhe}^2)$. To overcome this, we decompose the total temperature response into the local self-interaction term Ψ_{self} and a global field-interaction term Ψ_{inter}, defined in (21)-(22).

Both terms rely on the horizontal response function $\mathcal{R}$, which exhibits a local maximum at $\tau_{\max} = \frac{r^2}{4\alpha}$. This duration corresponds to the moment of peak thermal impact at a radial distance $r > 0$. At the borehole radius $r = r_b (\approx 75\ \text{mm})$, the thermal response is almost

instantaneous. For larger distances, such as the minimum BHE spacing $r \geq \Delta_{\min}(\approx 5\ \mathrm{m})$, the soil's thermal inertia acts as a low-pass filter: high-frequency fluctuations (e.g., hourly peaks) are significantly dampened and delayed by the time they reach neighboring boreholes. However, while individual pulses are preserved, the continuous injection or extraction of heat leads to a long-term thermal accumulation. During long operational times, these energy flows accumulate, leading to a gradual shift of the temperature distribution that eventually influences the performance of the entire BHE field.

Based on this spectral separation, we employ a dual-grid approach. For Ψ_{inter} we aggregate the load q onto a coarse grid (e.g., monthly averages). The convolution is performed on this reduced set of time steps, and the resulting smooth temperature curve is interpolated back to the hourly grid. For Ψ_{self} on the other hand, we perform the convolution on the original fine grid (hourly) to capture peak responses accurately. However, assuming uniform geometry of each BHE, this calculation is performed only once rather than for every pair of BHEs.

Finally, both Ψ_{self} and Ψ_{inter} can be cast as discrete convolutions. By utilizing the Fast Fourier Transform (FFT) and the Convolution Theorem, we reduce the complexity to $O(N_t \log N_t)$. For a 20-year hourly simulation, this reduces the operation count by several orders of magnitude, enabling the optimization of the BHE depth described in the following Section.

3. OPTIMIZATION METHODOLOGY

3.1 Algorithm Overview

Our optimization strategy takes advantage of the fact that spatial density and required borehole length are linked in a physical way. To keep the total drilling depth and installation cost as low as possible, it is best to give each borehole as much thermal storage space as possible. We do this with a two-step algorithm:

1) The algorithm puts a set number of BHEs inside the polygon that defines the property. The goal is to make the distance between any two boreholes and between any borehole and the property border as large as possible.

2) With the BHE positions fixed, we perform a PDE-constrained optimization to determine the minimum uniform length L along the BHE field. Using the analytical solution for the heat equation based on the FLS model, we identify the smallest L required to satisfy the prescribed thermal demand while ensuring that the resulting fluid temperatures remain within predefined operational limits throughout the entire simulation period.

3.2 Heuristic Positioning with Lloyd's algorithm

The spatial distribution objective described in Step 1 is formally framed as an optimization problem within the domain of Voronoi tessellations. Specifically, we seek to achieve a Centroidal Voronoi Tessellation (CVT) (Du et al., 1999) over the restricted, potentially non-convex domain Ω representing the property boundary. By characterizing the problem through its objective function (25) and associated constraints (26)-(28), we ensure the optimal dispersion of BHEs. With a set number of BHEs N_b that represent the desired number of Voronoi cells and a compact non-empty domain $\Omega \subset \mathbb{R}^2$, the goal is to find a set of N_b generators (centroids) $\{z_i\}_{i=1}^{N_b} \subset \Omega$ and their corresponding Voronoi cells $\{V_i\}_{i=1}^{N_b}$ that minimize the following integral:

$$\min_{\mathbf{z},\mathbf{V}} \quad \mathcal{J}(\mathbf{z},\mathbf{V}) \coloneqq \sum_{i=1}^{N_b} \int_{V_i} \| z_i - x \|^2 \, dx$$

$$\begin{aligned} &\text{s.t.} \\ &z_i \in V_i \quad \text{for all } i = 1, \dots, N_b \\ &V_i \subset \Omega \quad \text{for all } i = 1, \dots, N_b \\ &\bigcup_{i=1}^{N_b} V_i = \Omega, \quad V_i^\circ \cap V_j^\circ = \emptyset \text{ for } i \neq j. \end{aligned} \qquad (25-28)$$

The cells V_i are thus defined as the regions in Ω closest to z_i:

$$V_i = \{x \in \Omega \mid \| z_i - x \|^2 \leq \| z_j - x \|^2 \ \text{ for all } j \neq i\}$$

For any given cell V_i, the point z_i that minimizes $\int_{V_i} \| z_i - x \|^2 \, dx$ is uniquely identified as the geometric centroid of V_i, given by $z_i = \fint_{V_i} x \, dx$.

Lloyd's algorithm (Lloyd, 1982) is an iterative algorithm employed to approximate CVT. It consists of two alternating steps:

1) Given the current set of generators $\{z_i\}$, the domain Ω is partitioned into Voronoi cells V_i. This step inherently satisfies the domain confinement constraint $V_i \subset \Omega$ by restricting the Voronoi regions to Ω.

2) Each generator z_i is updated to the geometric centroid of its respective cell V_i.

In many real-world situations, the geometric domain Ω may not be convex. Using Lloyd's algorithm for CVT directly in these kinds of domains is problematic because the geometric centroid of a restricted Voronoi cell V_i does not always lie within V_i, which results in the constraint (26) being violated. To address this issue, we implement an intuitive adjustment: if a computed centroid c_i is determined to be outside the domain Ω, we project c_i onto Ω. There always exists a closest point, but the closest point may not be unique. Even though there is a chance that the operation will not be unique, it is still considered "well-defined" in a practical sense. Libraries for computational geometry (e.g. shapely (Gillies et al., 2013)) are made to find the closest point. If a centroid c_i is outside of Ω, projecting it to the nearest point in Ω will bring it back into the feasible area, which is in line with the rule $z_i \in \Omega$.

To numerically approximate the CVT of a continuous domain Ω, it is discretised into a sufficiently large quantity of uniformly distributed sample points (Du et al., 1999). Let $\mathcal{P} = \{p_1, \dots, p_M\}$ be a dense set of sample points within Ω. The objective function $\mathcal{J}$ of the optimization problem (25) is then approximated as

$$\min_{\mathbf{z},\mathbf{S}} \tilde{\mathcal{J}}(\mathbf{z}, \mathbf{S}) = \sum_{i=1}^{N_b} \sum_{p_j \in S_i} \| z_i - p_j \|^2,$$

where $S_i \subset \mathcal{P}$ are discrete sets of sample points forming a partition of $\mathcal{P}$. The constraints are then applied to this discrete formulation, requiring $z_i \in \Omega$.

The modified Lloyd's algorithm, adapted for this discrete setting and incorporating the centroid projection, is described in **Algorithm 1**.

The iterative refinement process of the Modified Lloyd's Algorithm on the non-convex L-shaped domain Ω with a hole is illustrated in **Figure 2**, showcasing the evolution of generators and their associated Voronoi cells over several key steps.

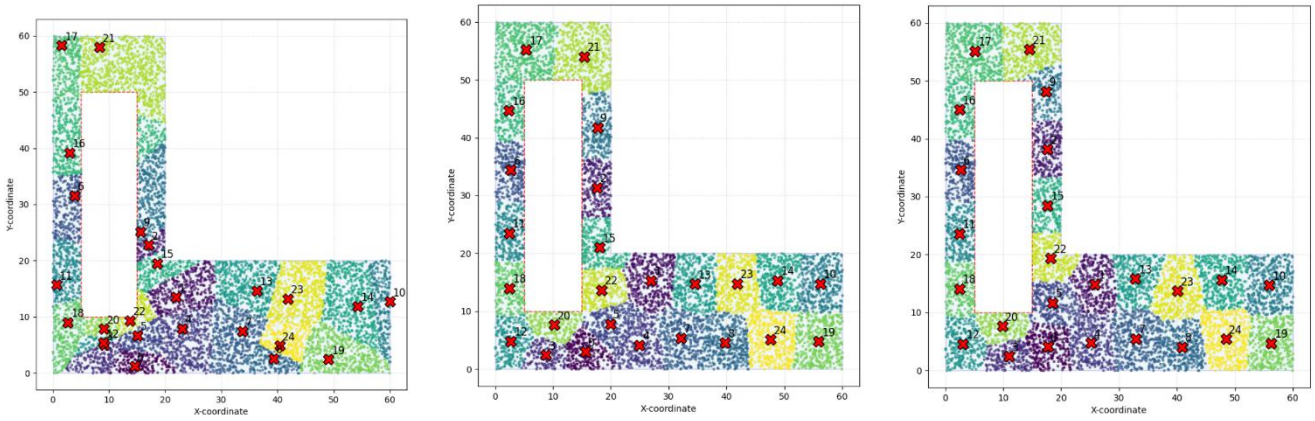

(a) Iteration 1 (b) Iteration 20 (c) Final State (Iteration 83)

Figure 2: Progression of the Modified Lloyd's Algorithm in a non-convex domain Ω. Sub-figure (a) shows the initial clustering, (b) demonstrates the state after 20 iterations as generators approach equilibrium, and (c) presents the final converged configuration of the generators and their corresponding Voronoi cells.

3.3 BHE Length Optimization

The subsequent analysis focuses on optimizing the vertical dimension, building on the optimized spatial arrangement of BHEs that was generated applying the Modified Lloyd's Algorithm in the previous section. Specifically, we aim to determine the optimal uniform depth for these pre-positioned BHEs.

Let us introduce the optimization problem:

$$\begin{aligned} \min_{L} \quad & L \\ \text{s.t.} \quad & T_{\min} \le T_{\text{out}}(t; L) \le T_{\max} \quad \forall t \in [0, \mathcal{T}] \\ & L \in [L_{\min}, L_{\max}] \end{aligned} \qquad (29-31)$$

The objective function (29) is a scalar-valued linear function that aims to minimize the total cost associated with BHE installation. The uniform borehole length for all BHEs is represented by the decision variable L.

Algorithm 1 Modified Lloyd's Algorithm for CVT in a Non-Convex Domain

Require: Non-convex domain $\Omega \subset \mathbb{R}^d$, number of generators N, maximum iterations K , convergence tolerance $\varepsilon > 0$.

Ensure: Set of converged generators $\{z_1, \ldots, z_N\}$.

Discretization of Ω: Generate a dense set of M uniformly distributed sample points $\mathcal{P} = \{p_1, \ldots, p_M\}$ such that $p_j \in \Omega$ for all $j = 1, \ldots, M$.
Initialization of Generators: Randomly select N initial generators $\{z_1^{(0)}, \ldots, z_N^{(0)}\}$ from $\mathcal{P}$.
for $t = 0, 1, \ldots, K-1$ **do**
    Assignment Step:
    Initialize empty discrete Voronoi cells $S_i^{(t)}$ for $i = 1, \ldots, N$.
    for each sample point $p_j \in \mathcal{P}$ **do**
        Determine the closest generator $z_k^{(t)}$ to p_j using Euclidean distance:
        $k^* = \text{argmin}_{k \in \{1,\ldots,N\}} \|z_k^{(t)} - p_j\|^2$
        Assign p_j to the corresponding discrete Voronoi cell: $S_{k^*}^{(t)} \leftarrow S_{k^*}^{(t)} \cup \{p_j\}$
    end for
    Update Step:
    for $i = 1, \ldots, N$ **do**
        if $S_i^{(t)}$ is not empty **then**
            Calculate the geometric centroid (mean) $c_i^{(t+1)}$ of $S_i^{(t)}$:
            $c_i^{(t+1)} = \frac{1}{|S_i^{(t)}|} \sum_{p_j \in S_i^{(t)}} p_j$
            Projection onto Ω:
            if $c_i^{(t+1)} \notin \Omega$ **then**
                $z_i^{(t+1)} \in \text{argmin}_{x \in \Omega} \|c_i^{(t+1)} - x\|^2$ ▷ Project $c_i^{(t+1)}$ to any of the nearest points in Ω
            else
                $z_i^{(t+1)} = c_i^{(t+1)}$
            end if
        else
            $z_i^{(t+1)} = z_i^{(t)}$ ▷ Generator remains in place if its cell is empty
        end if
    end for
    Convergence Check:
    if $\sum_{i=1}^{N} \|z_i^{(t+1)} - z_i^{(t)}\|^2 < \varepsilon$ **then**
        break
    end if
end for
return $\{z_1^{(t+1)}, \ldots, z_N^{(t+1)}\}$

The problem is subject to several constraints. The control constraint (31) sets practical limits on the length of the borehole L. The state constraints in (30) are crucial for making sure that the system operates properly by keeping the outlet fluid temperature from the BHEs, T_{out}, within a certain range of temperatures, $[T_{\text{min}}, T_{\text{max}}]$, for all times $t \in [0, \mathcal{T}]$. For numerical implementation, this continuous-time constraint is discretized over a finite set of time steps $\{t_l\}_{l=0}^{N_t-1}$ spanning the simulation period $\mathcal{T}$, leading to the practical form

$$T_{\text{out}}(t_l; L) \leq T_{\text{max}} \quad \text{and} \quad T_{\text{out}}(t_l; L) \geq T_{\text{min}} \quad \forall l = 0, \ldots, N_t - 1.$$

As explained in Section 2.4, the computation of T_{out} implicitly takes into account the building's thermal demand profile. This demand determines the dynamic heat extraction or injection rates from the BHE field, which directly affects the temperature of the fluid flowing out of the BHE field.

This optimization problem, featuring a linear objective, bound constraints, and non-linear state constraints, can be solved by various numerical optimization solvers. We use the Sequential Least Squares Programming (SLSQP) algorithm in Python's scipy.optimize (Virtanen et al., 2020) framework for our work. This choice is based on the fact that it performs well for medium-sized problems, handles both bound and non-linear constraints, and can be easily integrated into an open source development environment, making it a simple procedure to find a local optimum.

4. CASE STUDY

To demonstrate our proposed heuristic approach, we present a case study with two scenarios. The thermal building loads (Figure 3) for both scenarios are derived from a representative building model included in the TESS library (Thermal Energy System Specialists, 2024). The remaining parameters characterizing the fluid, soil, and borehole geometry are adopted from the literature (Bernier, 2006; Ahmadfard and Bernier, 2019), and are comprehensively detailed in **Table 1**. We will present the robustness of the heuristic approach by considering different property geometries, specifically the non-convex nature of the available land area for BHE placement.

Table 1: Key Fluid, Soil, and Borehole Geometry Properties for BHE Simulation.

Property	Symbol	Value	Unit
Fluid Properties			
Specific Heat Capacity	c_p	4019	J kg^{-1} K^{-1}
Density	ρ	1026	kg m^{-3}
Volumetric Heat Capacity	c_v	4.12 × 10^6	J m^{-3} K^{-1}
Mass Flow Rate	$\dot{m}$	10.34	kg s^{-1}
Volume Flow Rate	$\dot{V}$	0.01	m^3 s^{-1}
Thermal Conductivity	λ_f	0.468	W m^{-1} K^{-1}
Dynamic Viscosity	μ	0.00337	kg m^{-1} s^{-1}
Soil Properties			
Boundary Temperature	T_s	15	°C
Initial Inlet Temperature	$T_{in,0}$	15	°C
Thermal Conductivity	λ_s	1.9	W m^{-1} K^{-1}
Thermal Diffusivity	α_s	0.08	m^2 d^{-1}
Volumetric Heat Capacity	C_s	2.05 × 10^6	J m^{-3} K^{-1}
Borehole Geometry			
Borehole Diameter	D_b	150	mm
Pipe Distance (center-to-center)	w	83	mm
Outer Radius Pipe (in)	$r_{p,i}$	16.7	mm
Outer Radius Pipe (out)	$r_{p,o}$	16.7	mm
Pipe Wall Thickness	b_p	3.7	mm

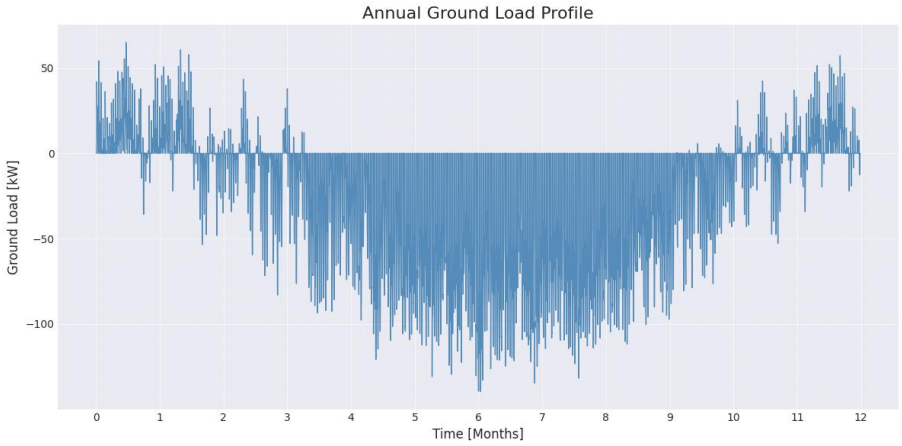

Figure 3: Annual Ground Load Profile with Hourly Discretization. This profile indicates how much thermal energy the BHE system must exchange at each hourly time interval over the period of a year. Positive values mean that heat is being extracted (heating demand), while negative values mean that heat is being rejected (cooling demand).

We define a benchmark configuration that will serve as a baseline for comparison. The setup has 25 BHEs arranged in a standard 5 x 5 grid with 8 m of space between each of them on a 1600 m^2 rectangular domain. This symmetrical layout is typical for a manual setup of sizing tools. The performance of the heuristic approach is first evaluated by comparing the benchmark 5 × 5 grid (**Figure *4***) with the

positions generated by the Modified Lloyd's Algorithm for the equivalent $1600\,\mathrm{m}^2$ domain (**Figure *5***b) over a 20-year simulation period ($N_t = 175{,}200 = 8760\,\mathrm{h/y} \times 20\,\mathrm{y}$). The proximity between these configurations is significant, with an average distance of only $1.96\,\mathrm{m}$ between the heuristically placed BHEs and their closest neighbors in the benchmark grid. This strong correlation indicates that under symmetric geometric constraints, the algorithm inherently reconstructs a quasi-grid structure, validating its ability to recover near-optimal placements in regular domains.

The optimization results using SLSQP confirm this further: the optimal length for the manual grid is $L^* = 91.47\,\mathrm{m}$, and the optimal length for the heuristic placement is $L^* = 91.44\,\mathrm{m}$. **Figure *3*** shows that this building's thermal demand is mostly for cooling. Because of this imbalance, the ground temperature rises over time, and the outlet temperature T_{out} reaches the upper operational limit T_{max} at the end of the 20-year simulation period, as shown in **Figure *6***.

The main benefit of the suggested heuristic lies in the fact that it can easily adjust to various domain constraints where manually fitting a grid is not straightforward. We examined the sensitivity of the optimal depth to the available property area by scaling the rectangle to $1024\,\mathrm{m}^2$ (**Figure *5***a) and $2304\,\mathrm{m}^2$ (**Figure *5***c).

The results, shown in **Table 2**, indicate there is a clear inverse relationship between the amount of space available and the depth of the borehole required. The algorithm employs the extra space in the "Large" scenario to maximize BHE separation, thereby decreasing thermal interference and allowing for a lower optimal depth of 84.07 m. On the other hand, the "Small" scenario needs a significant rise in depth to 101.86 m to compensate for the higher thermal interference.

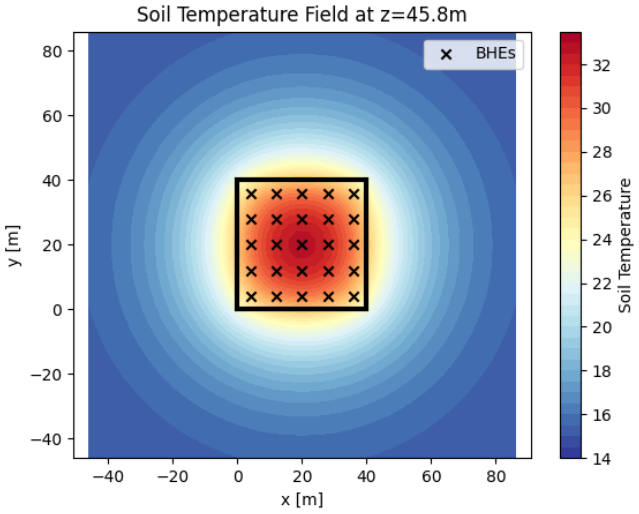

Figure 4: Soil temperature distribution at BHE mid-depth after a 20-year simulation period. Black crosses denote the positions of the BHEs, and the rectangle indicates the property boundary. The temperature field exhibits symmetric diffusion, consistent with the symmetry of the BHE array and the property borders, with the highest thermal accumulation concentrated around the centroid of the BHE field.

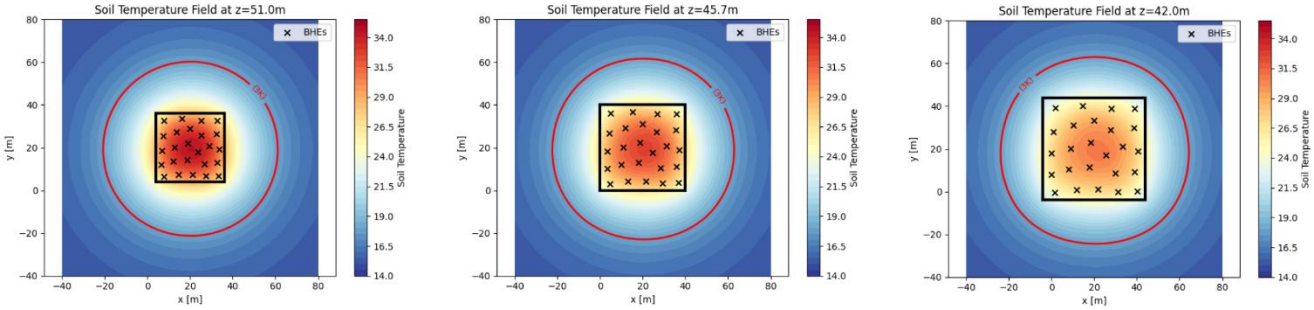

(a) $1024\,\mathrm{m}^2$ (Small) (b) $1600\,\mathrm{m}^2$ (Medium) (c) $2304\,\mathrm{m}^2$ (Large)

Figure 5: Soil temperature distribution at BHE mid-depth for varying property dimensions. A clear correlation is observed between property size and thermal saturation, with peak temperatures increasing as the property area is constrained. In all cases, the red contour line delineates a temperature increase of 3 K relative to the initial ground temperature.

Table 2: Optimal BHE Length L^* across various property geometries and scales.

	Grid (5x5)	Rect. (Medium)	Rect. (Small)	Rect. (Large)	L-Shape
Optimal Length (m)	91.47	91.44	101.86	84.07	80.72

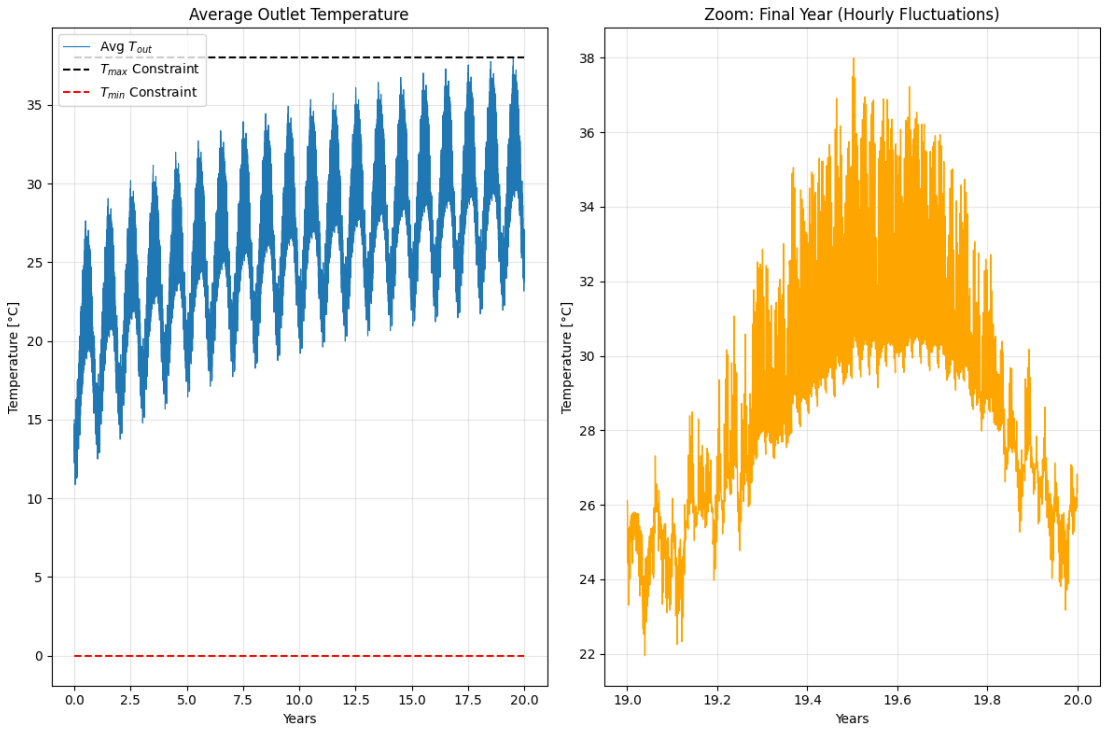

Figure 6: Evolution of the BHE outlet temperature over a 20-year horizon. The oscillating seasonal demand is superimposed on a rising mean temperature, eventually activating the T_{max} constraint.

To perform additional stress tests on the algorithm, we looked at a complicated L-shaped property with a rectangular exclusion zone that represents a building footprint. The Modified Lloyd's Algorithm effectively distributed the BHEs in the remaining non-convex area while considering the interior boundary. **Figure *7*** displays the resulting soil temperature field. Despite the irregular geometry, the heuristic successfully identifies a configuration that maintains the fluid temperature within the required bounds, resulting in an optimal length of 80.72 m.

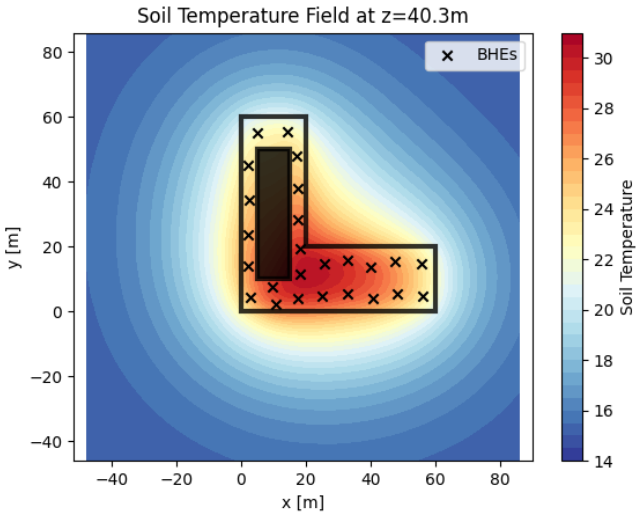

Figure 7: Soil temperature distribution in a non-convex L-shaped domain with an interior exclusion zone (building footprint). The algorithm automatically shifts BHE positions to optimize heat diffusion in the restricted space.

5. CONCLUSION AND OUTLOOK

We developed a quick, coupled analytical framework which utilizes a modified Lloyd's algorithm to find the optimal uniform depth for BHEs while also taking into account their spatial positioning. The heuristic effectively manages irregular and non-convex property boundaries, demonstrating its robustness in scenarios where traditional grid-based manual placement methods are impractical or inefficient. The main advantage of our method lies in its computational efficiency, enabling robust preliminary designs. The efficiency is achieved through a simple coupling of the Finite Line Source model with the inner 1D borehole heat transfer model, and the robustness through a modification of Lloyd´s algorithm for non-convex domains. Future research will explore gradient-based optimization methods for BHE coordinate positioning, going beyond the heuristic Lloyd's algorithm. This involves determining the gradients of the constraints in relation to BHE coordinates so that more rigorous gradient-descent algorithms can be used for spatial optimization. Another future improvement is to add explicit constraints on the maximum change in soil temperature (ΔT_{soil}) to the optimization problem. It is crucial to keep the ground from freezing or overheating, which can lower system efficiency, damage the ground over time, and violate regulatory guidelines. By including these features in the future, the presented framework can evolve into an even more powerful and accurate tool for the sustainable design of geothermal energy systems.

CONFLICT OF INTEREST

The authors declare no conflicts of interest.

ACKNOWLEDGEMENT

The work presented in this paper was supported by the German Federal Ministry of Economics and Climate Protection (BMWK) within the scope of the research project OptiGeoS (01256700/1).

Nomenclature

Calligraphic letters

$\mathcal{G}$	Green's Function
$\mathcal{R}$	Horizontal Kernel
$\mathcal{T}$	Simulation end time [s]
$\mathcal{Z}$	Vertical Kernel

Latin letters

N_b	Number of Boreholes [-]
R	Resistance
c	Specific heat capacity [J/(kg · K)]
L	Length of the Boreholes [m]
$\dot{m}$	Flow rate [kg/s]
p	Positions of BHE [-]
q	Heat extraction rate per unit length [W/m]
r_b	Borehole radius
T	Temperature [K]
x, y	Horizontal coordinates [-]
z	Vertical coordinate [-]

Greek letters

β	Normalized borehole conductance [-]
ρ	Density [kg/m^3]
γ	Borehole Characteristic parameter [-]
Ψ	Local/Global Field Interaction term [K]
λ	Thermal Conductivity [W/(m K)]
α	Thermal diffusivity [m^2/s]

Subscripts and superscripts

$^\circ$	interior of a set
$k, \hat{k}$	Counter for BHEs
r	Refrigerant
inter	pipe-to-pipe connection
s	soil-to-pipe connection

REFERENCES

M. Ahmadfard, M. Bernier, A review of vertical ground heat exchanger sizing tools including an inter-model comparison, Renewable and Sustainable Energy Reviews 110 (2019) 247–265.

M. A. Bernier, Closed-loop ground-coupled heat pump systems, Ashrae Journal 48 (2006) 12–25.

H. S. Carslaw, J. Jaeger, L. R. Ingersoll, O. J. Zobel, A. C. Ingersoll, J. Van Vleck, Conduction of heat in solids and heat conduction, Physics Today 1 (1948) 24–24.

M. Cimmino, M. Bernier, A semi-analytical method to generate g-functions for geothermal bore fields, International Journal of Heat and Mass Transfer 70 (2014) 641–650. URL: https://www.sciencedirect.com/science/article/pii/ S0017931013009915. doi:https://doi.org/10.1016/j.ijheatmasstransfer.2013.11.037.

H.-J. Diersch, D. Bauer, W. Heidemann, W. Rühaak, P. Schätzl, Finite element modeling of borehole heat exchanger systems: Part 1. fundamentals, Computers and Geosciences 37 (2011) 1122–1135. URL: https://www.sciencedirect.com/science/article/pii/S0098300410003055. doi:https://doi.org/10.1016/j.cageo.2010.08.003.

H.-J. G. Diersch, FEFLOW: Finite Element Modeling of Flow, Mass and Heat Transport in Porous and Fractured Media, Springer Berlin Heidelberg, Berlin, Germany, 2014. doi:10.1007/978-3-642-38739-5.

Q. Du, V. Faber, M. Gunzburger, Centroidal Voronoi tessellations: Applications and algorithms, SIAM Review 41 (1999) 637–676. URL: https://doi.org/10.1137/S0036144599352836. doi:10.1137/S0036144599352836. arXiv:https://doi.org/10.1137/S0036144599352836.

P. Eskilson, Thermal analysis of heat extraction boreholes, in: Proceedings of the 3rd International Conference on Energy Storage, KTH Royal Institute of Technology, 1987, pp. 1–10.

P. Eskilson, J. Claesson, Simulation model for thermally interacting heat extraction boreholes, Numerical Heat Transfer 13 (1988) 149–165. URL: https://doi.org/10.1080/10407788808913609. doi:10.1080/10407788808913609. arXiv:https://doi.org/10.1080/10407788808913609.

L. C. Evans, Partial differential equations, volume 19, American mathematical society, 2022.

G. A. Florides, S. A. Kalogirou, Ground heat exchangers—a review of systems, applications and sustainability issues, Renewable Energy 32 (2007) 2461–2478.

S. Gillies et al., The shapely user manual, URL https://pypi. org/project/Shapely (2013).

S. Halilovic, F. Böttcher, S. C. Kramer, M. D. Piggott, K. Zosseder, T. Hamacher, Well layout optimization for groundwater heat pump systems using the adjoint approach, Energy Conversion and Management 268 (2022a) 116033. doi:10.1016/j.enconman.2022.116033.

S. Halilovic, L. Odersky, T. Hamacher, Integration of groundwater heat pumps into energy system optimization models, Energy 238 (2022b) 121607. doi:10.1016/j.energy.2021.121607.

S. Halilovic, F. Böttcher, K. Zosseder, T. Hamacher, Optimization approaches for the design and operation of open-loop shallow geothermal systems, Advances in Geosciences 62 (2023a) 57–66.

S. Halilovic, F. Böttcher, K. Zosseder, T. Hamacher, Optimizing the spatial arrangement of groundwater heat pumps and their well locations, Renewable Energy 217 (2023b) 119148. doi:10.1016/j.renene.2023.119148.

S. Halilovic, F. Böttcher, K. Zosseder, T. Hamacher, Spatial analysis of thermal groundwater use based on optimal sizing and placement of well doublets, Energy 304 (2024) 132058.

G. Hellström, Thermal analysis of boreholes for seasonal storage of solar energy, Lund University, Department of Building Physics, 1995.

S. P. Kavanaugh, C. Orio, Design and installation of geothermal heat pump systems, ASHRAE Journal 50 (2008) S2–S12.

L. Lamarche, B. Beauchamp, A new contribution to the finite line-source model for geothermal boreholes, Energy and Buildings 39 (2007) 188–198. URL: https://www.sciencedirect.com/science/article/pii/S0378778806001824. doi:https://doi.org/10.1016/j.enbuild.2006.06.003.

S. P. Lloyd, Least squares quantization in pcm, IEEE Transactions on Information Theory 28 (1982) 129–137. doi:10.1109/TIT.1982.1056489.

N. Molina-Giraldo, P. Blum, K. Zhu, P. Bayer, Z. Fang, A moving finite line source model to simulate borehole heat ex-changers with groundwater advection, International Journal of Thermal Sciences 50 (2011) 2506–2513. URL: https://www.sciencedirect.com/science/article/pii/S129007291100192X. doi:https://doi.org/10.1016/j.ijthermalsci.2011.06. 012.

W. Peere, T. Blanke, Ghetool: An open-source tool for borefield sizing in python, Journal of Open Source Software 7 (2022) 4406. URL: https://doi.org/10.21105/joss.04406. doi:10.21105/joss.04406.

L. Rybach, W. Eugster, Geothermal energy: A renewable resource for heating and cooling, Energy 35 (2010) 2899–2908.

B. Sanner, G. Hellström, Earth energy designer, a software for calculating borehole heat exchangers; Earth energy designer, eine Software zur Berechnung von Erdwaermesondenanlagen, Geothermische Energie 18/19 (1997) 11–14.

M. Santos, et al., Decentralized control for connected heterogeneous teams of agents, IEEE Robotics and Automation Letters 4 (2019).

J. Spitler, J. Cook, X. Liu, Recent experiences calculating g-functions for use in simulation of ground heat exchangers, in: GRC Transactions, volume 44, Geothermal Resources Council, Virtual, Online, 2020, pp. 296–315. URL: https://www.osti.gov/biblio/1737649, geothermal Resources Council Virtual Annual Meeting and Expo.

J. D. Spitler, S. E. G. Gehlin, Borehole heat exchangers: An overview, Applied Thermal Engineering 86 (2015) 1–9.

Thermal Energy System Specialists, TESS Component Libraries for TRNSYS, Thermal Energy System Specialists (TESS), Madison, WI, USA, 2024. URL: https://www.trnsys.com/tess-libraries/, accessed: January 2024.

P. Virtanen et al., SciPy 1.0 Contributors, SciPy 1.0: Fundamental Algorithms for Scientific Computing in Python, Nature Methods 17 (2020) 261–272. doi:10.1038/s41592-019-0686-2.

M. Wetter, W. Zuo, T. S. Nouidui, X. Pang, Modelica Buildings library, Journal of Building Performance Simula-tion 7 (2014) 253–270. URL: https://doi.org/10.1080/19401493.2013.765506[AddtoCitaviprojectbyDOI]. doi:10.1080/19401493.2013.765506.

JC. Yavuzturk, J. D. Spitler, A long-term ground heat exchanger model for use with energy simulation programs, ASHRAE Transactions 105 (1999) 475–484.

L. Zhu et al., Voronoi-based coverage control for wireless sensor networks with limited communication ranges, IEEE Access 9 (2021).